

Representation Learning and Adversarial Generation of 3D Point Clouds

Panos Achlioptas* Olga Diamanti Ioannis Mitliagkas Leonidas Guibas

Department of Computer Science
Stanford University

Abstract

Three-dimensional geometric data offer an excellent domain for studying representation learning and generative modeling. In this paper, we look at geometric data represented as point clouds. We introduce a deep autoencoder network for point clouds, which outperforms the state of the art in 3D recognition tasks. We also design GAN architectures to generate novel point-clouds. Importantly, we show that by training the GAN in the latent space learned by the autoencoder, we greatly boost the GAN’s data-generating capacity, creating significantly more diverse and realistic geometries, with far simpler architectures. The expressive power of our learned embedding, obtained without human supervision, enables basic shape editing applications via simple algebraic manipulations, such as semantic part editing and shape interpolation.

1 Introduction

Deep learning architectures like autoencoders (AEs) [RHW88, KW13] and Generative Adversarial Networks (GANs) [GPAM⁺, RMC15, DCF⁺15, CLJ⁺16], are successful at learning complex data representations and generating realistic samples. Applied predominantly on natural image synthesis [DCF⁺15, IZZE16, LTH⁺16, NYB⁺16] and unsupervised learning [RMC] with impressive results, GANs are an object of intense research in the machine learning community. Other modalities like text, video and audio have also been studied to some extent [RAY⁺16, ZXL⁺16, VPT16, YZWY16]. In this paper we focus on a largely unexplored modality in the context of generative modeling: three-dimensional shape data.

Object-centered 3D data offer a great modality for exploration and analysis of generative modeling and encoding algorithms: they are a relatively pure form of input focused on largely single objects, as opposed to e.g. image data, where background clutter, and occlusions interact, introducing many semantic interpretation challenges. We argue that, of all the available digital representations of objects, 3D models are the closest to the actual physical object they represent. In contrast, the content of an image conforms to the geometry of the sensor, not that of meaningful semantic entities in the world. 3D data have already attracted research interest - see [ICNK] for references.

An important choice when working with 3D geometric input is the representation used to encode the information, eg. view-based projections [SMKL, WHC⁺, KAMC], volumetric grids [QSN⁺, WSK⁺] and graphs [BZSL, HBL, DBV, YSGG]. We choose point clouds as the input modality for studying latent representations and generative models. Point clouds are an expressive and compact representation of surface geometry, easily amenable to geometric operations, and more homogeneous compared to mesh

*Correspondence to: Panos Achlioptas <optas@cs.stanford.edu>.



Figure 1: Editing parts in point clouds using vector arithmetic on the AE latent space. Left to right: tuning the appearance of cars towards the shape of convertibles, adding armrests to chairs, removing handle from mug.

representations. These properties make them attractive from a learning point of view. In addition, given that the input to many visual computing applications is often a range-scanned point set representing an object or scene, any deep learning pipeline able to directly operate on raw points could bring a natural advantage.

An issue that any GAN-based pipeline needs to tackle is the fact that training GANs is notoriously hard. Optimizing the adversarial objective [GPAM⁺] is an inherently unstable saddlepoint-seeking process [GBC16], at the heart of which lies the min-max game played by a generator and a discriminator network. The instability is exacerbated by the fact that GANs are typically tasked with *jointly* learning a complex representation on top of this unstable adversarial game. Such architectures, referred to here as *monolithic GANs*, remain the norm and can be difficult to train [SGZ⁺16]. Some deep architectures work as GAN components and others do not. Even something seemingly innocuous like enabling batch normalization may throw off the training process. In a common failure mode, *mode collapse*, the discriminator is perfect, but the generator misses part of the actual data space. To avoid mode collapse, careful tuning and monitoring of the training process is considered essential and requires time and manual effort.

We build an end-to-end pipeline for 3D point clouds that uses an AE to create a latent representation, and a GAN to generate new samples in that latent space. Our AE is designed with a structural loss tailored to unordered point clouds. Our learned latent space, while compact, has excellent class-discriminative ability: per our classification results, it outperforms recent GAN-based representations by 4.3%. In addition, the latent space allows for vector arithmetic, which we apply in a number of shape editing scenarios, such as interpolation and structural manipulation.

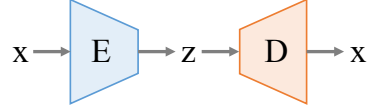
We argue that jointly learning the representation and training the GAN is unnecessary for our modality. We propose a workflow that first learns a representation by training an AE with a compact bottleneck layer, then trains a plain GAN in that fixed latent representation. One benefit of this approach is that AEs are a mature technology: training them is much easier and they are compatible with more architectures than GANs. We point to theory [AB17] that supports this idea, and verify it empirically: we show that GANs trained in our learned AE-based latent space generate visibly improved results, even with a generator and discriminator as shallow as a single hidden layer. Within a handful of epochs, we generate geometries that are recognized in their right object class at a rate close to that of ground truth data. Importantly, we report significantly better diversity measures (10x divergence reduction) over the state of the art, establishing that we cover more of the original data distribution. In summary, we contribute

- An effective *cross-category* AE-based latent representation on point clouds.
- The first (monolithic) GAN architecture operating on 3D point clouds.
- A surprisingly simpler, state-of-the-art GAN working in the AE’s latent space.

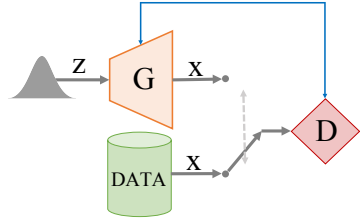
2 Preliminaries

In this section we give some background and introduce the basic building blocks for our work.

Autoencoders. Autoencoders (AE - inset) are deep architectures that aim to reproduce their input. They are especially useful, when they contain a narrow *bottleneck layer* between input and output. Upon successful training, the bottleneck layer corresponds to a low-dimensional representation, a *code* for the dataset. The Encoder (E) learns to compress a data point \mathbf{x} into its latent representation, \mathbf{z} . The Decoder (D) can then reproduce \mathbf{x} from its encoded version \mathbf{z} .



Generative Adversarial Networks. GANs are the state of the art in generative models. The basic architecture (inset) is based on an adversarial game between a *generator* (G) and a *discriminator* (D). The generator aims to synthesize samples that look indistinguishable from real data (drawn from $\mathbf{x} \sim p_{\text{data}}$) by passing a randomly drawn sample $\mathbf{z} \sim p_z$ through the generator function G . The discriminator tries to tell synthesized from real samples.



The most commonly used losses for the discriminator and generator networks are:

$$J^{(D)}(\boldsymbol{\theta}^{(D)}, \boldsymbol{\theta}^{(G)}) = -\mathbb{E}_{\mathbf{x} \sim p_{\text{data}}} \log D(\mathbf{x}) - \mathbb{E}_{\mathbf{z}} \log (1 - D(G(\mathbf{z}))) , \quad (1)$$

$$J^{(G)}(\boldsymbol{\theta}^{(D)}, \boldsymbol{\theta}^{(G)}) = -\mathbb{E}_{\mathbf{z} \sim p_z} \log D(G(\mathbf{z})) , \quad (2)$$

where $\boldsymbol{\theta}^{(D)}, \boldsymbol{\theta}^{(G)}$ are the parameters for the discriminator and the generator network respectively.

Challenges specific to point cloud geometry. Point clouds as an input modality present a unique set of challenges when building a network architecture. As an example, the convolution operator – now ubiquitous in image-processing pipelines – requires the signal (in our case, geometry) to be defined on top of an underlying grid-like structure. Such a structure is not available in raw point clouds, which renders them significantly more difficult to encode than e.g. images or voxel grids. Recent classification work on point clouds (PointNet [QSMG]) bypasses this issue by circumventing 2D convolutions altogether. Another issue with point clouds is that they are an unordered representation - permuting a set of points still describes the same shape. This complicates comparisons between two point sets, which would typically be needed as part of a loss function. This unordered-ness of point clouds also creates the need for making the encoded feature permutation invariant.

Point-set distances. Two permutation-invariant metrics for comparing unordered point sets have been proposed in the literature [FSG]. On the one hand, the *Earth Mover's distance* (EMD) [RTG] is the solution of a transportation problem which attempts to transform one set to the other. For two equally sized subsets $S_1 \subseteq R^3, S_2 \subseteq R^3$, their EMD is defined by

$$d_{EMD}(S_1, S_2) = \min_{\phi: S_1 \rightarrow S_2} \sum_{x \in S_1} \|x - \phi(x)\|_2. \quad (3)$$

where ϕ is a bijection. Interpreted as a loss, EMD is differentiable almost everywhere. On the other hand, the (still differentiable but more computationally efficient) *Chamfer* (pseudo)-distance (CD) involves assigning each point in one set to its nearest neighbor in the other set.

$$d_{CH}(S_1, S_2) = \sum_{x \in S_1} \min_{y \in S_2} \|x - y\|_2^2 + \sum_{y \in S_2} \min_{x \in S_1} \|x - y\|_2^2. \quad (4)$$

3 Autoencoder-based Representation Learning for Point Clouds

We start by describing our autoencoder design, tailored to 3D point clouds. The input to our AE network is a point cloud with 2048 points (2048×3 matrix), representing a 3D shape. Our source for shapes is the ShapeNet repository [CFG⁺]. We pre-center all shapes into a sphere of diameter 1.

Instead of avoiding convolutions altogether, as done in PointNet [QSMG], we exploit the fact that the models in ShapeNet within a given class can be pre-aligned to allow convolutions. We notice that in this case, a simple lexicographic ordering of the point coordinates is sufficient to impose an approximate neighborhood structure on the point set. This allows us to apply convolutions in groups of neighboring points, instead of treating each point independently, as in [QSMG]. The combination of the lexicographic order in conjunction with the pre-alignment of shapes also lifts the requirement for explicitly imposing permutation invariance on the feature: the ordered point clouds for similar and pre-aligned shapes are likely to roughly correspond. We found that reasoning within groups of points leads to significantly better autoencoding reconstruction error. For instance, we observed better preservation of high-frequency geometric detail at the output of the decoder.

The encoder architecture follows the principle of [SDBR]: convolution layers followed by ReLUs, with increasing strides. The last convolution layer is followed by a column-wise maximum to produce a 512-dimensional vector which is the basis for our latent space. The decoder passes this 512 dimensional variable through 3 connected layers with ReLUs, to produce the 2048×3 output. We used the efficient EMD-distance approximation [FSG] as our structural loss, to cope with the lack of order in the point cloud. We found that EMD tends to be faithful to a human’s perception of geometric differences between shapes, much more so than some image-based losses. We believe this constitutes another advantage of clean point cloud input.

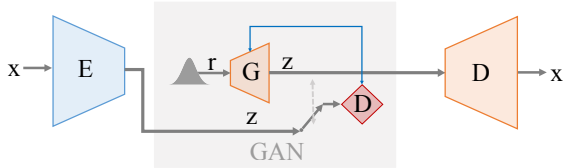
Different AE setups (denoising/regularised) brought no noticeable advantage over our “vanilla” architecture. We suspect this is due to the presence of a number of fairly similar shapes in our dataset, which, due to sampling, are represented in the AE input by slightly different point sets. In a sense this perhaps simulates the effect of adding noise to the input, as is done in a denoising AE.

4 Generative Networks for Point Clouds

In this section we introduce a GAN architecture tailored to point-cloud data. Then we propose a more efficient pipeline that first trains an AE and trains a much smaller GAN in the learned latent space.

Raw point cloud GAN (r-GAN). The first version of our generative model operates directly on the raw 2048×3 point set input — to the best of our knowledge this work is the first to present a GAN for point clouds. For the purposes of this manuscript, we refer to this generative model as *r-GAN*. The architecture of the discriminator consists of a set of MLP-layers similar to [QSMG] with leaky ReLUs [MHN13], followed by a dropout layer [SHK⁺] and then a set of fully connected layers leading to the final sigmoid output of the discriminator. The generator takes as input a 512-dimensional noise vector and proceeds by mirroring the structure of the AE decoder to map the input into a 2048×3 output.

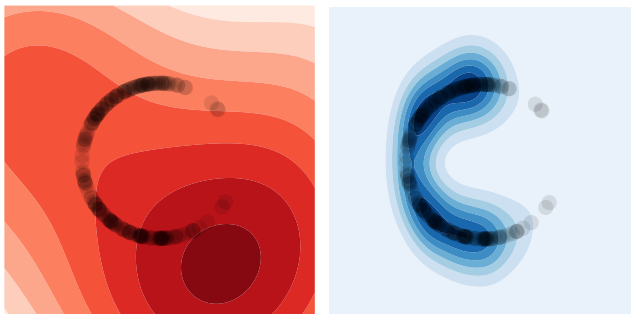
Latent-space GAN (l-GAN). In our latent-space GAN (here, *l-GAN*), instead of operating on the raw point cloud input, we pass the data through our pre-trained autoencoder, trained separately for each object class with the EMD loss function. Both the generator and the discriminator of the GAN then operate on the 512-dimensional bottleneck variable



of the AE. Finally, once the GAN training is over, the output of the generator is decoded to a point cloud via the AE decoder. The architecture for the l-GAN is *significantly* simpler than the one of the r-GAN. We found that very shallow designs for both the generator and discriminator (in our case, 1 hidden layer for the generator and 2 for the discriminator) are sufficient to produce realistic results.

Intuition. There are a number of reasons why we would want to use this factored architecture, which separates representation from generation. AEs are a *mature and stable* tool: training an AE to learn a complex representation is considered an easy task that does not require much tuning and monitoring. Training a big GAN, on the other hand, is very demanding in terms of computer (and man) hours. Another advantage of using an AE to learn the representation, is the *freedom to select a good structural metric*. This proves to be particularly important in our modality (see Section 5.1). In order to train a GAN, we need to use one of the established GAN objectives, losing out on potential opportunities for domain-specific structure. Similarly, there are fewer restrictions in the architectures that can be used in a workable AE.

Finally, training a GAN in the latent space is *much faster* and *much more stable*. The inset provides some intuition with a toy example, where the data live in a 1D circular manifold. The density in red is the result of training a GAN’s generator in the original, 2D, data space. The most commonly used GAN objectives are equivalent to minimizing the JSD between the generator and data distributions. Unfortunately, the JSD is part of a family of divergences that become unbounded when there is *support mismatch*, which is the case in the example: the GAN places a lot of mass *outside* the data manifold. On the other hand, when training a small GAN in the *fixed* latent space of a trained AE (blue), the overlap of the two distributions increases significantly. According to recent theoretical advances [AB17] this should improve stability.



5 Experimental Evaluation

5.1 Evaluating the latent representation

A common technique for evaluating the quality of unsupervised representation learning algorithms is to apply them as a feature extractor on supervised datasets and evaluate the performance of linear models fitted on top of these features. We use this technique to evaluate the performance of the latent “features” computed by our AE. For this experiment to be meaningful, the AE was trained across all different shape categories: we used 57,000 models from ShapeNet from 55 categories of man-made objects. To obtain features for an input 3D shape, we feed forward to the network its point-cloud and extract the 512-dimensional bottleneck layer vector. This feature is then processed by a linear classification SVM trained on the de-facto 3D classification benchmark of ModelNet [WSK⁺]. Table 1 shows comparative results. Note that previous state of the art [WZX⁺] uses several layers of a GAN to derive a 7168-long feature; our 512-dimensional feature is more intuitive and parsimonious.

Recall (Section 1) that our decoupling of latent representation from generation allows flexibly choosing the AE loss, which can improve the learned feature. On ModelNet10, which includes primarily larger objects than ModelNet40, an AE trained with the EMD loss performs slightly better than one trained with the CD. On the other hand, when the variation within the collection increases, CD produces better results. This is perhaps due to its more discrete nature, which allows it to understand rough edges and

| Method | MN40 | MN10 |
|------------------------------------|--------------|--------------|
| SPH [Kazhdan et al., 2003] | 68.2% | 79.8% |
| LFD [Chen et al., 2003] | 75.5% | 79.9% |
| T-L Network [Girdhar et al., 2016] | 74.4% | - |
| VConv-DAE [Sharma et al., 2016] | 75.5% | 80.5% |
| 3D-Gan [Wu et al., 2016] | 83.3% | 91.0% |
| ours, EMD loss | 84.4% | 95.3% |
| ours, CD loss | 85.7% | 95.0% |

Table 1: Classification performance on ModelNet40 and ModelNet10. All methods train a linear SVM based on features derived in an unsupervised fashion.

high frequency geometric details. Finally, note that since our AEs were not trained on ModelNet, this experiment also demonstrates the domain-robustness of our learned features.

5.2 Evaluating the GANs

We train an adversarial network for each of the five major object categories of ShapeNet (chairs, sofas, tables, cars and airplanes), each containing 3.5-7K models. The AEs used for the l-GANs were trained using the EMD loss, which was found to create more aesthetically pleasing results than the CD.

Evaluating and interpreting probabilistic generative models is a genuinely hard task which has attracted much attention recently [TvdOB]. Quantitative measurements based on empirically estimated log-likelihoods have been shown to poorly capture the efficacy of generative methods. Saliman et al. [SGZ⁺16] introduced the inception score, which correlates well with how a human would evaluate the realism of synthetic images. Inspired by the inception score, we leverage a classification network to produce a confidence on how much our synthetic point-clouds belong to a given object’s class. We use PointNet [QSMG], which is the state of the art for classifying point clouds. At the other end of the spectrum, since GANs are often prone to mode-collapse, we also need to characterize how well they eventually cover the ground-truth distribution. For this we introduce two more evaluation metrics:

MMD. Minimum Matching Distance. For every 3D point-set in the ground-truth we find its closest point-set in the synthetic dataset. Closeness between point sets is computed using the Chamfer distance. We report the average of the minimum chamfer distances over all matched shape pairs as the final value. Reporting the CD also helps remove any bias from using the EMD as the structural loss for the AE’s.

JSD. The Jensen Shannon Divergence of empirically estimated random variables defined in 3D space. Our training data are pre-aligned in 3D space, and thus also the generated data; this allows measuring the degree to which the point clouds from the two distributions co-vary. To do this, we consider a 28^3 regularly-spaced voxel grid centered in the sphere of diameter 1. By counting the number of 3D points lying within each voxel, across all point clouds of either distribution, we can construct a 28^3 random variable vector for that distribution. We report the JSD of these two random vectors.

Both these measures detect mode collapse in the GAN output. Note that the relatively small training set size (compared to image datasets) allows us to sample the generator with the same number of data used for training, which reduces sampling uncertainty. Quantitative results are shown in Figure 2 for the *chair* category - additional results can be found in the supplemental material.

Comparisons to state-of-the-art. To the best of our knowledge we are the first to propose GANs on point-cloud data. To find out how our models fare against other 3D generative methods, we compare

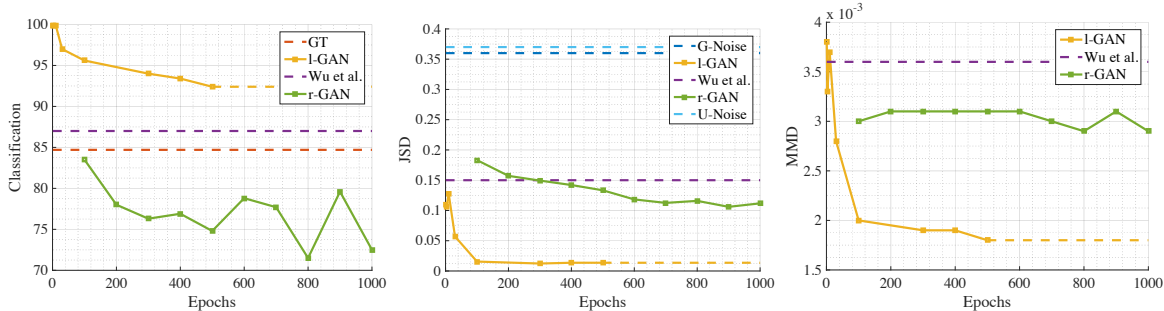


Figure 2: Evaluating the GAN architectures on the *chair* dataset. The classification score (left) measures fidelity of the generated objects. GT denotes the average classification score attained by the ground-truth point clouds. J-S divergence / MMD (middle / right) measure diversity (smaller values indicate more diversity). For scale, we also plot the JS response to two random noise distributions (uniform and gaussian).

to a recent voxel-grid based approach [WZX⁺]. For comparisons, we convert their voxel grid output into a point-set with 2048 points, by performing farthest-point-sampling on the isosurface of the grid values. Per the authors’ suggestion, we used an isovalue parameter of 0.1 and isolated the largest connected component from the isosurface.

Discussion. The performance of r-GAN is generally better in terms of its diversity (as measured by JSD and MMD) to the state of the art method of Wu[WZX⁺], while also creating realistic-looking results, as shown by the classification score. On the other hand, the l-GAN outperforms all methods, both in terms of classification and diversity, and does so with significantly less training epochs (of the order of 50 or less). It’s also worth noting that the training time for one epoch of the l-GAN is approximately an order of magnitude smaller than for the r-GAN, due to its much smaller architecture and dimensionality. Our better MMD and JSD scores indicate that the l-GAN is more robust to mode collapse. Finally, the behaviour of the r-GAN, especially in terms of classification, is noticeably more unstable; as argued in Section 1, this showcases a typical issue that arises when training GANs.

For fairness, we acknowledge that since [WZX⁺] operates on voxel grids, it is not necessarily on equal standing when it comes to generating point clouds. Additionally, the PointNet classifier was trained on ShapeNet, and [WZX⁺] often generates shapes that only rarely appear in ShapeNet. In conjunction with their higher tendency for mode collapse, this partially accounts for the lower classification scores commonly obtained by this method (see supplemental material E.2).

5.3 Effect of latent space size on GAN training

In this experiment, we demonstrate that training a GAN in a smaller latent space is faster. Furthermore, we show that, at least in our modality, training a GAN in a small latent space yields generative distributions that are as good—as measured by JSD—as the distributions of GANs trained in bigger latent spaces. This result complements our experiments in Section 5.2, where we evaluate the raw GAN (r-GAN) and latent GAN (l-GAN) on task-specific metrics, and further motivates the use of pre-trained AEs in this domain. Specifically, we fully train AEs with size 32, 64, 128, 256, 512 and fix the resulting models and latent spaces. Then we evaluate the JSD between the learned generative distribution and the data distribution, throughout GAN training in those latent spaces. We repeat this experiment both for a vanilla GAN, but also for WGAN-GP [GAA⁺17], to demonstrate that the effect we describe are also present in state-of-the-art, stable generative models. The results, as seen in Figure 3, suggest that in our modality, pre-training an AE to get a small latent space and using it to train a small

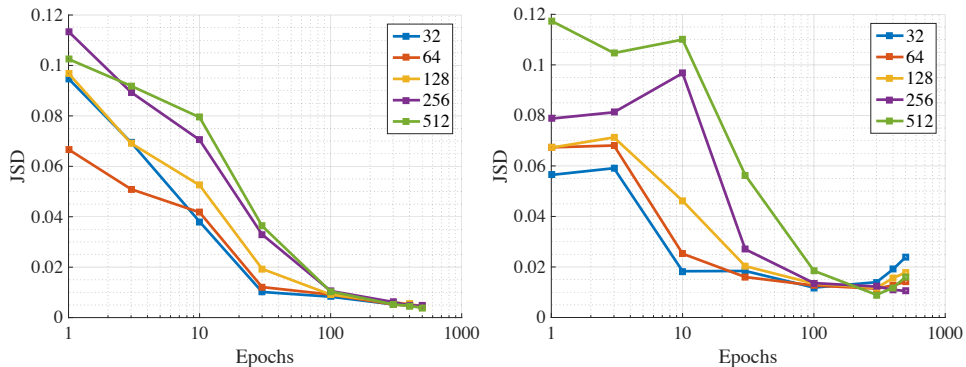


Figure 3: Training WGAN-GPs [GAA⁺17] (left) and vanilla GANs (right) on the chair class in the latent space of fully trained, fixed AEs with bottlenecks of size 32, 64, 128, 256, 512. Lower JSD values signal that the GAN distribution is closer to the data distribution. The results show that working in a fixed, small latent space, speeds up GAN training without sacrificing fidelity as measured by JSD.

GAN is the most efficient way to get a generative model. In this experiment we do not control for the varying representational capacity of the AEs. In Section E we repeat the same experiment, but use early stopping to ensure all AEs yield the same EMD loss.

5.4 Applications of the latent space representation

For shape editing applications, we use the embedding we learned with the EMD-AE trained *across all* 55 object classes, not separately per-category. This showcases its ability to encode features for different shapes, and enables interesting applications involving different kinds of shapes.

Editing shape parts. We use the shape annotations of Yi et al. [YKC⁺] as guidance to modify shapes. As an example, assume that a given object category (e.g. chairs) can be further subdivided into two sub-categories \mathcal{A} and \mathcal{B} : every object $A \in \mathcal{A}$ possesses a certain structural property (e.g. has armrests, is four-legged, etc.) and objects $B \in \mathcal{B}$ do not. Using our latent representation we can model this structural difference between the two sub-categories by the difference between their average latent representations $\mathbf{x}_{\mathcal{B}} - \mathbf{x}_{\mathcal{A}}$, where $\mathbf{x}_{\mathcal{A}} = \sum_{A \in \mathcal{A}} \mathbf{x}_A$, $\mathbf{x}_{\mathcal{B}} = \sum_{B \in \mathcal{B}} \mathbf{x}_B$. Then, given an object $A \in \mathcal{A}$, we can change its property by transforming its latent representation: $x_{A'} = x_A + \mathbf{x}_{\mathcal{B}} - \mathbf{x}_{\mathcal{A}}$, and decode $\mathbf{x}_{A'}$ to obtain $A' \in \mathcal{B}$. This process is shown in Figure 1. Note that the volume of chairs with armrests is on average 10% larger than the chairs without, which is reflected in the output of this process.

Interpolating shapes. By linearly interpolating between the latent representations of two shapes and decoding the result we obtain intermediate variants between the two shapes. This produces a “morph-like” sequence with the two shapes at its end points (Figure 4). Our latent representation is powerful enough to support removing and merging shape parts, which enables morphing between shapes of significantly different appearance. Our cross-category latent representation enables morphing between shapes of different types, c.fg. the second row for an interpolation between a bench and a sofa. More results are available in the additional material.



Figure 4: Interpolating between different point clouds, using our latent space representation. Note the interpolation between structurally and topologically different shapes.

5.5 Generative results

We show some results using our latent-space GANs in Figure 5. We noticed that l-GAN produces crisper and less noisy results than the r-GAN; demonstrating another advantage of using a good structural loss on the decoupled, pre-trained AE.

6 Related Work

Recent work [SGZ⁺16] gives some useful techniques that help training the classic monolithic GAN. They propose feature matching as a method of regularizing the training process and ameliorating mode collapse issues. Variational autoencoders (VAEs) [KW13] learn a representation compatible with a given prior distribution. They are more stable than GANs, though the reported results seem to be of lower quality (i.e. slightly blurry images [GBC16]). VAEGANs [LSLW15] improve upon VAEs by training a VAE jointly with a GAN. DCGANs and LAPGANs [RMC15, DCF⁺15] involve training of models of increasing level of detail, making training a bit smoother. MDGANs introduce regularizers in the GAN objective meant to prevent mode collapse and improve the stability of training [CLJ⁺16]. WGANs [ACB17] are a very elegant and intuitive solution to the problem of vanishing gradients and mode collapse. They optimize an objective based on the Wasserstein distance between the data and generator distributions, which is known to be more stable and yield good results.

All of the GAN variants above improve the vanilla GAN in some way, but all are nonetheless monolithic. Perhaps closer to our training workflow approach are the following results:



Figure 5: Generative results using our latent-space GAN. Note the variability and fidelity of the result.

- The “plug and play” generative architecture [NYB⁺16] essentially uses some pretrained components, which allows for substituting a core “condition” network that guides a pretrained generator. This kind of network is currently considered state of the art for image generation, though it involves a number of complex steps (e.g. Langevin sampling). Our proposed AE+GAN workflow is much simpler and seems to be a great fit for the point-cloud modality.
- Adversarial autoencoders [MSJ⁺15] use a GAN in the latent space of an AE. However they are still trained *jointly*.
- GMMNs [LSZ15] are an alternative to GANs. They only train a generator and use a moment-matching objective to bring the generator distribution close to the data distribution. One of the proposed variants involves training in the latent space of an already training AE, similarly to our approach, which significantly improves performance. They have enjoyed limited adoption, likely due to the moment matching objective’s computational complexity - quadratic on the number of samples. This limits their applicability in high dimensions.
- Older work on sampling from autoencoders [RBDV12, BYAV13, BLAY14].

A number of recent works ([WZX⁺], [WXX⁺], [GFRG], [BLRW], [MWM], [ZWB⁺]) have explored generative and discriminative representations for geometry. They operate on different modalities,

typically voxel grids or view-based image projections. To the best of our knowledge, our work is the first to study such representations for point clouds.

7 Conclusion

In this work we present a compact AE-based representation for point cloud geometry, with the best known discriminative and expressive capacity. Combined with a GAN, this latent space can be used to produce synthetic point clouds, that are not only visually plausible but also diverse. We show that decoupling the GAN from the latent space representation enables greatly simplifying the GAN architecture, which in turn has significant advantages in terms of training effort as well as quality of results. We believe that this workflow is very intuitive and intend to explore its applicability on other modalities.

An interesting avenue for future work involves further exploring the idea of ingesting point clouds by sorting them lexicographically before applying a 1D convolution. A possibly interesting extension would be to study different 1D orderings that capture locality differently, e.g. Hilbert curves. We can also aim for convolution operators of higher order (2D and 3D).

References

- [AB17] Martin Arjovsky and Léon Bottou. Towards principled methods for training generative adversarial networks. In *NIPS 2016 Workshop on Adversarial Training. In review for ICLR*, volume 2016, 2017.
- [ACB17] Martin Arjovsky, Soumith Chintala, and Léon Bottou. Wasserstein gan. *arXiv preprint arXiv:1701.07875*, 2017.
- [BLAY14] Yoshua Bengio, Eric Laufer, Guillaume Alain, and Jason Yosinski. Deep generative stochastic networks trainable by backprop. In *International Conference on Machine Learning*, pages 226–234, 2014.
- [BLRW] André Brock, Theodore Lim, James M. Ritchie, and Nick Weston. Generative and discriminative voxel modeling with convolutional neural networks. *CoRR*.
- [BYAV13] Yoshua Bengio, Li Yao, Guillaume Alain, and Pascal Vincent. Generalized denoising auto-encoders as generative models. In *Advances in Neural Information Processing Systems*, pages 899–907, 2013.
- [BZSL] Joan Bruna, Wojciech Zaremba, Arthur Szlam, and Yann LeCun. Spectral networks and locally connected networks on graphs. *CoRR*.
- [CFG⁺] Angel X. Chang, Thomas A. Funkhouser, Leonidas J. Guibas, Pat Hanrahan, Qi-Xing Huang, Zimo Li, Silvio Savarese, Manolis Savva, Shuran Song, Hao Su, Jianxiang Xiao, Li Yi, and Fisher Yu. Shapenet: An information-rich 3d model repository. *CoRR*.
- [CLJ⁺16] Tong Che, Yanran Li, Athul Paul Jacob, Yoshua Bengio, and Wenjie Li. Mode regularized generative adversarial networks. *arXiv preprint arXiv:1612.02136*, 2016.
- [DBV] Michaël Defferrard, Xavier Bresson, and Pierre Vandergheynst. Convolutional neural networks on graphs with fast localized spectral filtering. In *Advances in Neural Information Processing Systems 29: Annual Conference on Neural Information Processing Systems 2016, December 5-10, 2016, Barcelona, Spain*, pages 3837–3845.
- [DCF⁺15] Emily L Denton, Soumith Chintala, Rob Fergus, et al. Deep generative image models using a laplacian pyramid of adversarial networks. In *Advances in neural information processing systems*, pages 1486–1494, 2015.
- [FSG] Haoqiang Fan, Hao Su, and Leonidas J. Guibas. A point set generation network for 3d object reconstruction from a single image. *CoRR*.
- [GAA⁺17] Ishaan Gulrajani, Faruk Ahmed, Martín Arjovsky, Vincent Dumoulin, and Aaron C. Courville. Improved training of wasserstein gans. *CoRR*, abs/1704.00028, 2017.
- [GBC16] Ian Goodfellow, Yoshua Bengio, and Aaron Courville. *Deep learning*. MIT Press, 2016.
- [GFRG] Rohit Girdhar, David F. Fouhey, Mikel Rodriguez, and Abhinav Gupta. *Learning a Predictable and Generative Vector Representation for Objects*, pages 484–499. Springer International Publishing, Cham.
- [GPAM⁺] Ian Goodfellow, Jean Pouget-Abadie, Mehdi Mirza, Bing Xu, David Warde-Farley, Sherjil Ozair, Aaron Courville, and Yoshua Bengio. Generative adversarial nets. In Z. Ghahramani, M. Welling, C. Cortes, N. D. Lawrence, and K. Q. Weinberger, editors, *Advances in Neural Information Processing Systems 27*, pages 2672–2680. Curran Associates, Inc.

- [HBL] Mikael Henaff, Joan Bruna, and Yann LeCun. Deep convolutional networks on graph-structured data. *CoRR*.
- [ICNK] Anastasia Ioannidou, Elisavet Chatzilari, Spiros Nikolopoulos, and Ioannis Kompatsiaris. Deep learning advances in computer vision with 3d data: A survey. *ACM Comput. Surv.*, (2):20:1–20:38, April.
- [IZZE16] Phillip Isola, Jun-Yan Zhu, Tinghui Zhou, and Alexei A. Efros. Image-to-image translation with conditional adversarial networks. *CoRR*, abs/1611.07004, 2016.
- [KAMC] Evangelos Kalogerakis, Melinos Averkiou, Subhransu Maji, and Siddhartha Chaudhuri. 3d shape segmentation with projective convolutional networks. *CoRR*.
- [KW13] Diederik P Kingma and Max Welling. Auto-encoding variational bayes. *arXiv preprint arXiv:1312.6114*, 2013.
- [LSLW15] Anders Boesen Lindbo Larsen, Søren Kaae Sønderby, Hugo Larochelle, and Ole Winther. Autoencoding beyond pixels using a learned similarity metric. *arXiv preprint arXiv:1512.09300*, 2015.
- [LSZ15] Yujia Li, Kevin Swersky, and Rich Zemel. Generative moment matching networks. In *Proceedings of the 32nd International Conference on Machine Learning (ICML-15)*, pages 1718–1727, 2015.
- [LTH⁺16] Christian Ledig, Lucas Theis, Ferenc Huszar, Jose Caballero, Andrew P. Aitken, Alykhan Tejani, Johannes Totz, Zehan Wang, and Wenzhe Shi. Photo-realistic single image super-resolution using a generative adversarial network. *CoRR*, abs/1609.04802, 2016.
- [MHN13] Andrew L. Maas, Awni Y. Hannun, and Andrew Y. Ng. Rectifier nonlinearities improve neural network acoustic models. In *Proceedings of the 30th International Conference on Machine Learning (ICML-13)*, 2013.
- [MSJ⁺15] Alireza Makhzani, Jonathon Shlens, Navdeep Jaitly, Ian Goodfellow, and Brendan Frey. Adversarial autoencoders. *arXiv preprint arXiv:1511.05644*, 2015.
- [MWM] Maierdan Maimaitimin, Keigo Watanabe, and Shoichi Maeyama. Stacked convolutional auto-encoders for surface recognition based on 3d point cloud data. *Artificial Life and Robotics*, pages 1–6.
- [NYB⁺16] Anh Nguyen, Jason Yosinski, Yoshua Bengio, Alexey Dosovitskiy, and Jeff Clune. Plug & play generative networks: Conditional iterative generation of images in latent space. *arXiv preprint arXiv:1612.00005*, 2016.
- [QSMG] Charles Ruizhongtai Qi, Hao Su, Kaichun Mo, and Leonidas J. Guibas. Pointnet: Deep learning on point sets for 3d classification and segmentation. *CoRR*.
- [QSN⁺] Charles Ruizhongtai Qi, Hao Su, Matthias Nießner, Angela Dai, Mengyuan Yan, and Leonidas J. Guibas. Volumetric and multi-view cnns for object classification on 3d data. In *2016 IEEE Conference on Computer Vision and Pattern Recognition, CVPR 2016, Las Vegas, NV, USA, June 27-30, 2016*, pages 5648–5656.
- [RAY⁺16] Scott E. Reed, Zeynep Akata, Xinchun Yan, Lajanugen Logeswaran, Bernt Schiele, and Honglak Lee. Generative adversarial text to image synthesis. In *Proceedings of the 33rd International Conference on Machine Learning, ICML 2016, New York City, NY, USA, June 19-24, 2016*, pages 1060–1069, 2016.

- [RBDV12] Salah Rifai, Yoshua Bengio, Yann Dauphin, and Pascal Vincent. A generative process for sampling contractive auto-encoders. *arXiv preprint arXiv:1206.6434*, 2012.
- [RHW88] David E Rumelhart, Geoffrey E Hinton, and Ronald J Williams. Learning representations by back-propagating errors. *Cognitive modeling*, 5(3):1, 1988.
- [RMC] Alec Radford, Luke Metz, and Soumith Chintala. Unsupervised representation learning with deep convolutional generative adversarial networks. *CoRR*.
- [RMC15] Alec Radford, Luke Metz, and Soumith Chintala. Unsupervised representation learning with deep convolutional generative adversarial networks. *arXiv preprint arXiv:1511.06434*, 2015.
- [RTG] Yossi Rubner, Carlo Tomasi, and Leonidas J. Guibas. The earth mover’s distance as a metric for image retrieval. *International Journal of Computer Vision*, (2):99–121.
- [SDBR] Jost Tobias Springenberg, Alexey Dosovitskiy, Thomas Brox, and Martin A. Riedmiller. Striving for simplicity: The all convolutional net. *CoRR*.
- [SGZ⁺16] Tim Salimans, Ian Goodfellow, Wojciech Zaremba, Vicki Cheung, Alec Radford, and Xi Chen. Improved techniques for training gans. In *Advances in Neural Information Processing Systems*, pages 2226–2234, 2016.
- [SHK⁺] Nitish Srivastava, Geoffrey Hinton, Alex Krizhevsky, Ilya Sutskever, and Ruslan Salakhutdinov. Dropout: A simple way to prevent neural networks from overfitting. *J. Mach. Learn. Res.*, (1):1929–1958, January.
- [SMKL] Hang Su, Subhransu Maji, Evangelos Kalogerakis, and Erik G. Learned-Miller. Multi-view convolutional neural networks for 3d shape recognition. In *2015 IEEE International Conference on Computer Vision, ICCV 2015, Santiago, Chile, December 7-13, 2015*, pages 945–953.
- [TvdOB] Lucas Theis, Aäron van den Oord, and Matthias Bethge. A note on the evaluation of generative models. *CoRR*.
- [VPT16] Carl Vondrick, Hamed Pirsiavash, and Antonio Torralba. Generating videos with scene dynamics. *CoRR*, abs/1609.02612, 2016.
- [WHC⁺] Lingyu Wei, Qixing Huang, Duygu Ceylan, Etienne Vouga, and Hao Li. Dense human body correspondences using convolutional networks. In *2016 IEEE Conference on Computer Vision and Pattern Recognition, CVPR 2016, Las Vegas, NV, USA, June 27-30, 2016*, pages 1544–1553.
- [WSK⁺] Zhirong Wu, Shuran Song, Aditya Khosla, Fisher Yu, Linguang Zhang, Xiaoou Tang, and Jianxiong Xiao. 3d shapenets: A deep representation for volumetric shapes. In *IEEE Conference on Computer Vision and Pattern Recognition, CVPR 2015, Boston, MA, USA, June 7-12, 2015*, pages 1912–1920.
- [WXX⁺] Yueqing Wang, Zhige Xie, Kai Xu, Yong Dou, and Yuanwu Lei. An efficient and effective convolutional auto-encoder extreme learning machine network for 3d feature learning. *Neurocomputing*, pages 988 – 998.
- [WZX⁺] Jiajun Wu, Chengkai Zhang, Tianfan Xue, Bill Freeman, and Josh Tenenbaum. Learning a probabilistic latent space of object shapes via 3d generative-adversarial modeling. In D. D. Lee, M. Sugiyama, U. V. Luxburg, I. Guyon, and R. Garnett, editors, *Advances in Neural Information Processing Systems 29*, pages 82–90. Curran Associates, Inc.

- [YKC⁺] Li Yi, Vladimir G. Kim, Duygu Ceylan, I-Chao Shen, Mengyan Yan, Hao Su, Cewu Lu, Qixing Huang, Alla Sheffer, and Leonidas J. Guibas. A scalable active framework for region annotation in 3d shape collections. *ACM Trans. Graph.*, (6):210:1–210:12.
- [YSGG] Li Yi, Hao Su, Xingwen Guo, and Leonidas J. Guibas. Syncspeccnn: Synchronized spectral CNN for 3d shape segmentation. *CoRR*.
- [YZWY16] Lantao Yu, Weinan Zhang, Jun Wang, and Yong Yu. Seqgan: Sequence generative adversarial nets with policy gradient. *CoRR*, abs/1609.05473, 2016.
- [ZWB⁺] Zhuotun Zhu, Xinggang Wang, Song Bai, Cong Yao, and Xiang Bai. Deep learning representation using autoencoder for 3d shape retrieval. *Neurocomputing*, pages 41 – 50. Big Learning in Social Media Analytics Containing a selection of papers from the 2014 International Conference on Security, Pattern Analysis, and Cybernetics (ICSPAC2014).
- [ZXL⁺16] Han Zhang, Tao Xu, Hongsheng Li, Shaoting Zhang, Xiaolei Huang, Xiaogang Wang, and Dimitris N. Metaxas. Stackgan: Text to photo-realistic image synthesis with stacked generative adversarial networks. *CoRR*, abs/1612.03242, 2016.

A AE Details

All autoencoders we built had the following architecture: The encoder was a 4-layer deep 1D-convolutional network followed by a max-pool layer. The output of the max-pool was treated as the latent/bottleneck vector of the AE. The number of filters, filter sizes and strides in each layer of the encoder were respectively: $\{128, 128, 256, 512\}$, $\{40, 20, 10, 10\}$ and $\{1, 2, 2, 1\}$.

The decoder was a 3-layer deep network, comprised by fully connected layers with $\{1024, 2048, 2048 \times 3\}$ neurons each. Each layer was followed by a batch-normalization layer, which was followed by a ReLU non-linearity. For the AE’s used in the reported GAN experiments (airplane, car, chair, sofa, table), we trained each AE for 1000 epochs with the EMD Loss. The AE used in the cross-class experiment of the entire ShapeNetCore, was trained for 2000 epochs. Also, for the cross-class AE a random rotation along the up-direction, was applied to every point-cloud within a batch. For training the autoencoders we used ADAM with an initial learning rate of 0.0005, beta-1 of 0.9 and batch size of 50.

B r-GAN Details

The discriminator consists of 10 layers in total, five MLPs, three Fully Connected (FCs), one drop-out and one max-pool. The first five layers are the MLPs with kernel sizes of $\{64, 128, 256, 256, 512\}$ each. The sixth layer is a drop-out with a 0.5 probability. The seventh layer is a max-pool. The last three FC layers have $\{128, 64, 1\}$, neurons each. The last single neuron is processed by a sigmoid function. The output of each MLP layer and the first two FC layers, is processed with batch-normalization which is followed by leaky-ReLU, with leak of 0.2 units. The generator consists of six fully connected layers with $\{64, 128, 256, 512, 1024, 2048 \times 3\}$ number of neurons each. We add a ReLU between each layer. Also, in the layer prior to the last one we add a dropout layer with probability of keeping a connection 0.5. This drop-out unit was active in both at training and test time. We trained r-GAN with ADAM with initial learning rate of 0.0001, and beta-1 of 0.5 in batches of size 50, for 1500 epochs. The noise vector was drawn by a spherical Gaussian of 512 dimensions with zero mean and 0.5 sigma.

C l-GAN Details

The discriminator consists of 3 fully connected layers with $\{256, 512, 1\}$ neurons each. We added ReLU and batch-normalization layers between the layers and a sigmoid after the last neuron. The generator consists of 2 fully connected layers with $\{128, 512\}$ neurons each. The output of both layers is processed by a ReLU and the output of the first layer only, by a batch-normalization. We trained l-GAN with ADAM with initial learning rate of 0.0001, and beta-1 of 0.9 in batches of size 50, for 500 epochs. The noise vector was drawn by a spherical Gaussian of 512 dimensions with zero mean and 0.5 sigma.

D SVM Parameters for Autoencoder Evaluation

We use a one-versus-all linear SVM classifier with an l_2 penalty and balanced class weights.

| Structural Loss | ModelNet40 | | | ModelNet10 | | |
|-----------------|-------------|---------------|---------------|-------------|---------------|----------|
| | scaling C | intercept I | loss L | scaling C | intercept I | loss L |
| EMD | 1 | 3 | squared hinge | 0.4 | 1 | hinge |
| CD | 0.6 | 1 | squared hinge | 1 | 4 | hinge |

Table 2: Training parameters of SVMs used in each dataset with each Structural Loss of the AE.

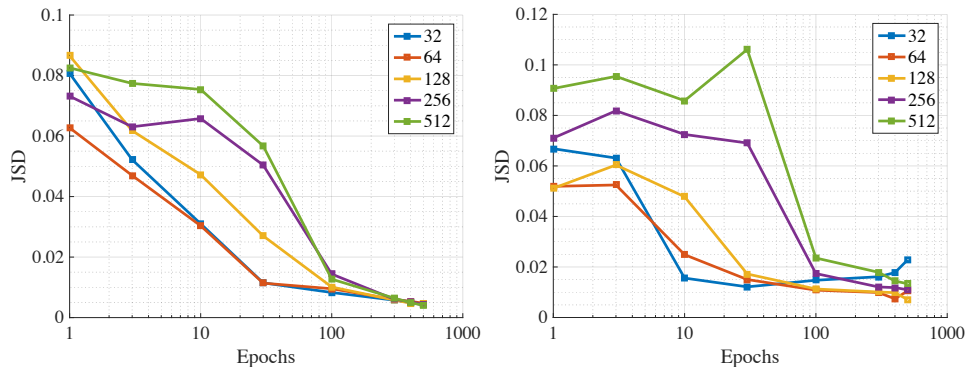


Figure 6: Training iwGANs (left) and vanilla GANs (right) on the chair class in the latent space of fixed AEs with bottlenecks of size 32, 64, 128, 256, 512. This experiment replicates the protocol used to produce Figure 3, with the following difference: we control for potential differences in the representational power of the different AEs. To do that, we perform early stopping during the AE training to ensure that all AE models achieve the exact same EMD loss. The results again show that working in a fixed, small latent space, makes GAN training faster without sacrificing fidelity as measured by JSD.

E Extra Experiments

In this section we include some experiments that did not make it to the main body, due to the space limitation.

E.1 Training GANs in small, fixed latent spaces

Here we repeat the GAN-training experiment from Section 5.2, with added control for variations in representational power of the AEs. Specifically, we pre-train AEs with size 32, 64, 128, 256, 512 and stop them when they achieve a common EMD loss (the minimum value achieved by all of them). Then we evaluate the performance of GAN training in those latent spaces. The results are presented in Figure 6.

E.2 Quantitative results on different object classes

Similarly to Figure 2, the plots in Figures 7,8,9 illustrate the efficacy of our approach for different object classes (*sofa*, *table* and *car*). In particular, note the better stability of the l-GAN, and its better performance compared to the baseline r-GAN, both in terms of classification and the diversity of results.

E.3 Further qualitative results

We show more shape editing results in Figures 10 and 11.

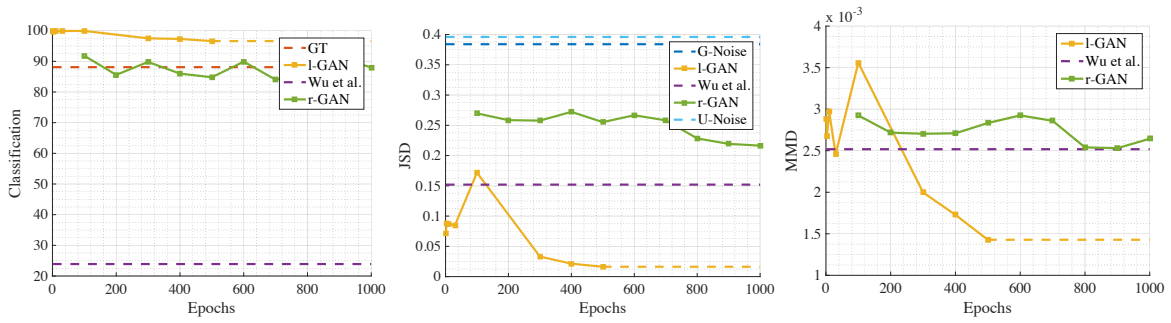


Figure 7: Evaluating the GAN architectures on the *sofa* dataset.

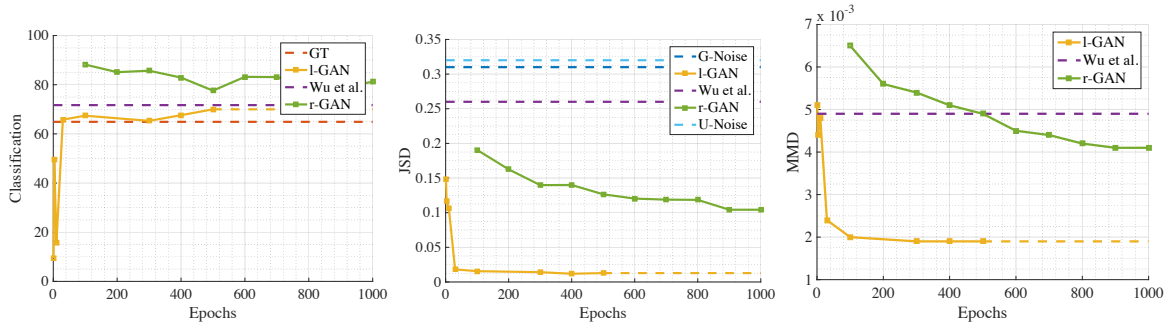


Figure 8: Evaluating the GAN architectures on the *table* dataset.

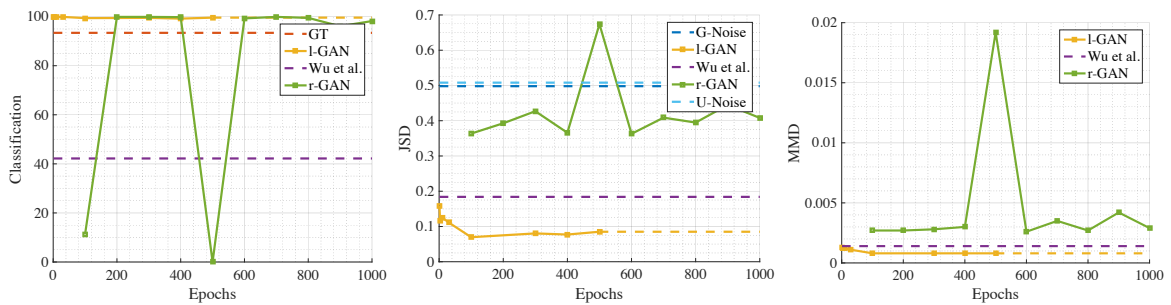


Figure 9: Evaluating the GAN architectures on the *car* dataset.

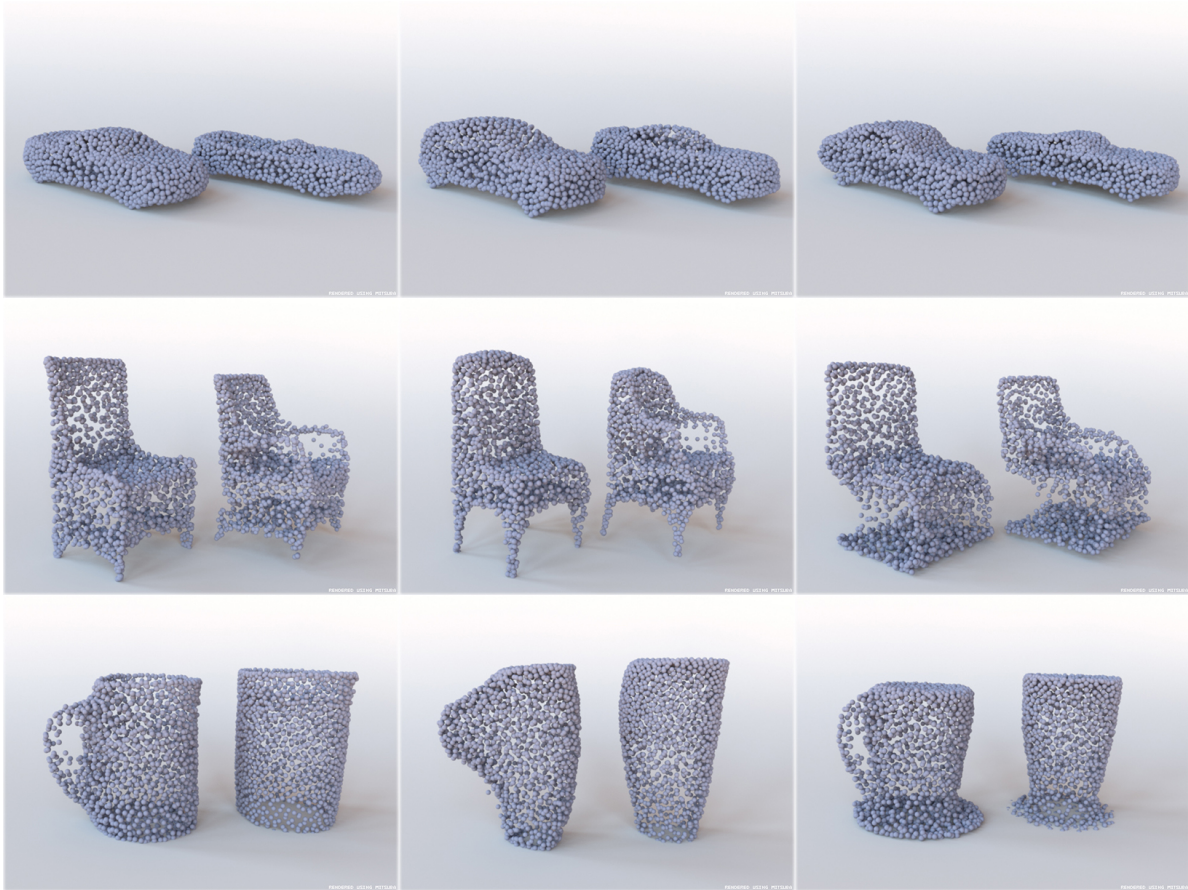


Figure 10: Additional shape editing results.



Figure 11: Additional shape interpolation results.